Part Based Bit Error Analysis of Iris Codes

I. Tomeo-Reyes*, V. Chandran

Queensland University of Technology, 2 George Street, Brisbane, Australia

Abstract

In order to effectively use iris patterns in biometric recognition, there is value in knowing how bit errors in iris codes are distributed. In this work, the iris is considered in a part-based framework as rings and sectors. A mean normalised bit error is defined as the bit error averaged over the entire part and over an ensemble of images. The distribution of this error for genuine comparisons is investigated as a function of radius (ring) and angle (sector) for a range of factors more comprehensively than previous studies of consistency of iris codes. Two iris recognition systems and three data sets are used. The effect of residual segmentation errors after automated segmentation is checked, and masks are manually refined to obtain segmentation error free data for further investigation. The effect of factors such as capture sensor, resampling, input iris image resolution, filter type and encoding scheme, and changes in pupil size is systematically investigated. Results confirm the finding in previous works that the pupillary and limbic boundaries are more error-prone than the middle region of the iris. This study further confirms that this V-shaped radial trend is not significantly disturbed by any of the above factors other than pupil size changes. Both pupil dilation and constriction result in increased bit errors which no longer show a dip in the middle region of the iris. The distribution of errors as a function of angle is approximately uniform regardless of the factor investigated but shows a small decrease towards the sectors near the eye corners.

*Corresponding author

Email addresses: `inma.tomeoreyes@qut.edu.au` (I. Tomeo-Reyes),
`v.chandran@qut.edu.au` (V. Chandran)

1. Introduction

The richness of the iris texture and its variability across individuals make it a very reliable biometric trait for personal authentication [1]. However, texture information within the iris is not uniform, and bits in an iris code differ in their consistency from one sample to another for the same identity.

Different approaches have been proposed to investigate the differences between regions of the iris in their contributions to iris recognition performance. An early approach by Pereira and Veiga [2] analysed all possible combinations of five out of ten concentric iris rings to improve the performance of an iris recognition system. If rings are numbered from the pupillary boundary out to the limbus as 1 to 10, the best performance was obtained when using rings 2, 3, 4, 5 and 7. To complete the analysis [3], they divided the iris into a greater number of concentric rings and used a genetic algorithm to determine those that led to the best performance. Results showed that the selected rings were mainly located in the central regions of the iris.

Hollingsworth *et al.* [4] demonstrated the existence of fragile or inconsistent bits, which are defined as bits that have a substantial probability of changing from a 0 to a 1 or vice versa in iris codes of the same iris. Given a number of test images, the percentage of images in which a particular bit of the iris code changes measures the inconsistency of that bit. A bit is said to be fragile at $p\%$ consistency threshold if it changes in at least $p\%$ of the images. Using a consistency threshold of 40%, best results were obtained for rings 5 to 12 out of twenty (or 2 to 6 out of ten approximately) for rings numbered in ascending order from the pupillary boundary out to the limbus. This information was exploited by masking the fragile bits before the comparison stage in order to increase the recognition accuracy. The authors of this work also found that certain bits are consistent even across out-of-focus and noisy images. Rathgeb *et al.* [5] used

the previous work as a reference and computed a mask in which the consistency at each bit position was defined as the difference between the estimated probabilities of occurrence of intra-class and inter-class errors. Tan and Kumar [6] exploited the temporal intra-class information in the feature space to derive a stability map which indicates the consistency of bits in iris codes.

Broussard *et al.* [7] and Hilal *et al.* [8] calculated the recognition accuracy achieved by different iris regions in order to evaluate their contribution to the comparison decision. In [7], rings 4 to 8 out of ten were reported to be the most consistent, whereas in [8], rings 2 and 3 out of ten performed the best, followed by rings 1, 4 and 5. In both cases rings are numbered in ascending order from the pupillary boundary out to the limbus.

Results reported in all previous approaches seem to indicate that texture information located in the central region of the iris is more consistent, and the maximum consistency is reached closer to the pupillary boundary than to the limbus. However, some differences exist in the results obtained for rings near the pupillary boundary which should be further investigated.

Inconsistencies in different regions of the iris could be influenced by factors other than texture information. Potential causes of inconsistencies, such as segmentation [4, 8], normalisation [8], template and filter size [7], filter type [4], and iris alignment [4] have been previously investigated considering different criteria. Fragile bits [4], probabilities of occurrence of intra-class and inter-class errors [5], recognition accuracy [7, 8] or decidability [8] are some of these criteria. Although experiments confirmed that these factors affect consistency, the lack of a common testing framework makes it difficult to compare the different effects in a quantitative manner. A methodology is proposed here to comprehensively analyse the consistency of bits of different iris regions including additional factors, such as changes in capture sensor, resampling parameters, resolution, and changes in pupil size.

In this work, irides are divided into radial partitions or rings as well as angular partitions or sectors for error analysis. Statistics of bit errors calculated using Hamming distance are computed for genuine and impostor distributions as

functions of radius and angle. The results provide insight into the most effective manner in which iris texture can be used considering the spatial distribution of bit errors in iris codes. Three data sets and two iris recognition systems are used in the experiments.

This paper is organized as follows. In Section 2, the proposed error analysis is described in detail. The data sets and iris recognition systems used in the experiments are described in Section 3. A list of factors that affect the distribution of bit errors within the iris is presented in Section 4, together with tests to quantify their effect. Conclusions are outlined in Section 5.

2. Proposed Error Analysis Method

An iris recognition system has four main stages: data acquisition, pre-processing, feature extraction, and comparison (see Fig. 1). Once a 2D image of the eye has been captured using an iris sensor, the iris region is isolated from other structures in its vicinity during the segmentation and masking stages. The resultant iris region is then unwrapped into a rectangular block of fixed dimensions during the normalisation stage. The normalised iris image is then subjected to filtering, and the ensuing phasor responses are encoded into a bit string referred to as an iris code. In the comparison stage, the dissimilarity between two iris codes is computed. The mask generated during the pre-processing stage is used to prevent degraded regions from being compared. Both the iris code and the mask can be viewed as binary vectors. It is assumed here that a mask value is 1 where a bit is retained and 0 where a bit is masked away.
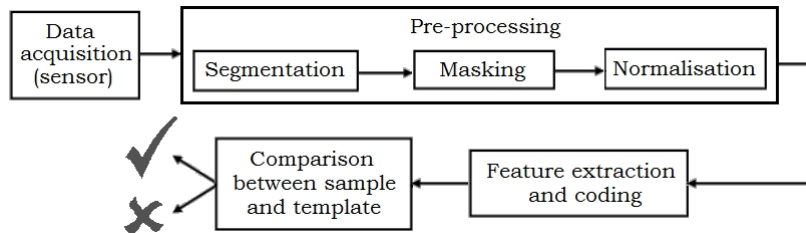

Figure 1: Typical stages of iris recognition.

The error analysis presented in this research is based on the number of bits that differ between the iris codes of different iris samples.

Different approaches can be used to implement the different stages of an iris recognition system. In this paper, the binary iris codes and masks required to compute the bit errors are obtained from two open source iris recognition systems, OSIRISv4.1 [9] and USITv1.0.3 [10]. Details of these systems are provided in Section 3.

The *normalised bit error* between two iris codes $\{\mathbf{C}1, \mathbf{C}2\}$ whose mask bit vectors are denoted $\{\mathbf{M}1, \mathbf{M}2\}$ is defined as the number of bits that differ between the unmasked portions of the iris codes as a fraction of the total number of bits that are compared. This dissimilarity metric is also known as normalised Hamming distance or fractional Hamming distance. The *normalised bit error* is calculated using equation (1), where $\oplus$ and $\&$ are the bitwise-XOR and the bitwise-AND operation respectively, and $||$ represents the L1 norm.

$$\epsilon = \frac{|(\mathbf{C}1 \oplus \mathbf{C}2) \ \& \ (\mathbf{M}1 \ \& \ \mathbf{M}2)|}{|\mathbf{M}1 \ \& \ \mathbf{M}2|} \tag{1}$$

The value of ϵ is computed for different iris parts (rings and sectors), obtained as functions of radius and angle. Radial partitioning results in R concentric rings of the same width and angular partitioning results in S sectors of equal size numbered as shown in Fig. 2. The iris code associated with each part is a fraction of the complete iris code, properly selected by masking. Since the number of bit errors is divided over the total number of bits that are compared, it is possible to use and compare filters that generate iris codes of different sizes from the same region.

Subscripts r and θ are used to denote, respectively, rings and sectors, and superscripts i and j are used to identify the specific ring ($i = 1, \ldots, R$) and sector ($j = 1, \ldots, S$). According to this notation, ϵ_r^i denotes the normalised number of bit errors in ring i, and ϵ_θ^j denotes the normalised number of bit errors in sector j. Since databases differ in the number of identities or users and the number of iris samples for each, the previously defined normalised number of

bit errors per ring and sector are averaged for the number of comparisons of any given database. The *mean normalised bit error* per ring and sector denoted $\bar{\epsilon}_r^i$ and $\bar{\epsilon}_\theta^j$ respectively, is thus calculated as the average of the normalised bit error for a region when computed over a number of samples. The *mean normalised bit error* can be used to identify the iris regions with higher consistency and thus contributing relatively more to better performance for genuine comparisons.
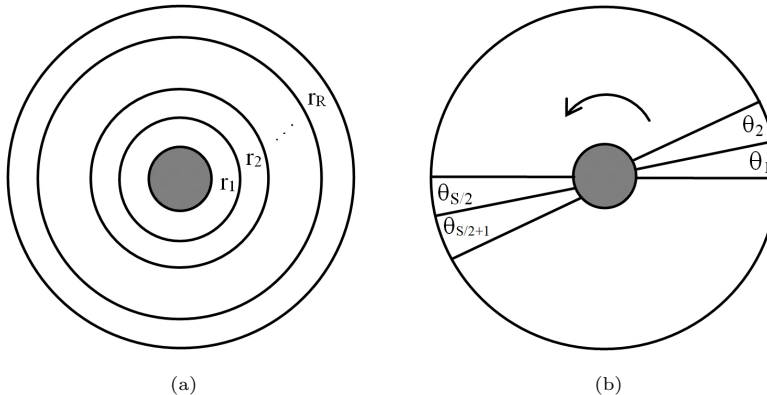

Figure 2: Iris partitioning. (a) Radial partitioning. (b) Angular partitioning.

3. Experimental Results

Three data sets and three iris recognition systems are used in the experiments to investigate the consistency of bits in iris codes. These are described in detail in this section. The mean normalised bit error calculated with equation (1) for different rings and sectors using a reference data set and iris recognition system is also analysed.

3.1. Iris Data Sets

Three different data sets are used to compute the mean normalised bit error. These are ICE 2005 [11], CASIA-IrisV4-Thousand [12] and an in-house data set known as Iris Degradations Data Set (IDDS). From these data sets, ICE 2005 is used as the reference in all the experiments.

6

3.1.1. ICE 2005

The ICE 2005 data set was provided by the National Institute of Standards and Technology (NIST) for the iris recognition challenge problem known as Iris Challenge Evaluation (ICE) 2005. It comprises a total number of 2953 iris images captured from 132 different participants at a resolution of 640×480 in the near infrared (NIR) wavelength. The data set includes images of right irides (1425 images from 124 users) and left irides (1528 images from 120 users), acquired at the same time in most cases. The sensor used for the data collection was the LG EOU 2200.

3.1.2. CASIA-IrisV4-Thousand

CASIA-IrisV4-Thousand contains 20000 iris images (10 images per eye) from 1000 subjects. All images are stored with resolution 640×480. The sensor used for the data collection was the IKEMB-100 camera by IrisKing, a dual-eye iris camera which works in the NIR wavelength. The main sources of intra-class variations are eyeglasses and specular reflections. The subset of CASIA-IrisV4-Thousand used in this work contains 500 users. Only the left iris images are used. After removing those images with eyeglasses, a total data subset of 3424 left iris images is obtained.

3.1.3. IDDS

The Iris Degradations Data Set or IDDS is an in-house database that includes a total of 2183 iris images acquired at a resolution of 640×480 using the iris sensor IG-AD100, a dual eye auto-focus camera which works in the NIR wavelength. The database is divided into four main subsets: images captured under normal conditions, images affected by quality degradation due to local noise (eyelid obstruction, gaze deviation and glasses), images affected by changes in pupil size, and images affected by occlusion. In this work only the images acquired under normal conditions and those affected by changes in pupil size are used (see Fig. 3).

– *Normal conditions (IDDS:NC).*

This subset includes a total of 354 iris images captured under normal conditions in a controlled environment (normal room illumination). Images were taken from 59 different participants who provided 3 images per eye. It is used to check the effect of the capture sensor on the distribution of bit errors.

– *Drug-induced and light-induced pupil dilation (IDDS:Dilation-drugs and IDDS:Dilation-light).*

The subsets used to check the effect of pupil dilation on the number and distribution of bit errors comprise 292 iris images captured from 38 different eyes. In the case of drug-induced dilation or mydriasis, the mydriatic agent tropicamide was instilled to participants in the form of eye drops. Images affected by light-induced pupil dilation were obtained by turning the ambient lighting off. The ratio between the pupil radius and the iris radius, or pupil-to-iris ratio, is higher than 0.515 for all irides affected by pupil dilation included in these subsets.

– *Drug-induced and light-induced pupil constriction (IDDS:Constriction-drugs and IDDS:Constriction-light).*

In order to analyse the effect of pupil constriction on the distribution of bit errors within the iris two subsets are used, which include 417 iris images captured from 69 different eyes. Drug-induced constriction or miosis was provoked by instillation of the miotic agent pilocarpine, whereas images affected by light-induced pupil constriction were obtained by pointing a visible light source directly at the participants' eyes. The pupil-to-iris ratio is lower than 0.265 for all irides affected by pupil constriction included in these subsets.

The analysis of factors other than segmentation should provide insight into bit errors that are directly related to the iris texture and its encoding, and should not be influenced by errors introduced owing to segmentation. For this reason, only trimmed data sets composed of images which are free from segmentation
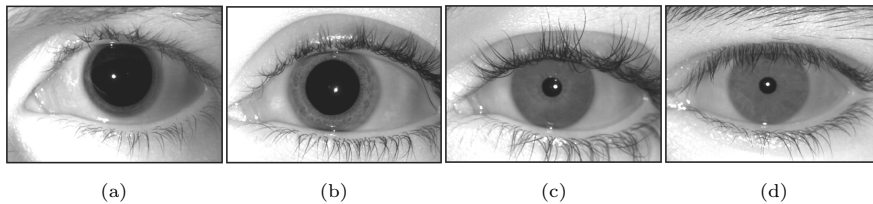
| (a) | (b) | (c) | (d) |

Figure 3: IDDS sample images affected by changes in pupil size with pupil-to-iris ratio (ρ) values. (a) Drug-induced dilation ($\rho = 0.75$), (b) light-induced dilation ($\rho = 0.58$), (c) light-induced constriction ($\rho = 0.22$), and (d) drug-induced constriction ($\rho = 0.20$).

errors are used in the experiments. Information on the segmentation-error-free data is summarized in Table 1.

Table 1: Size of segmentation-error-free subsets used in the experiments.

Data set	Iris classes	Images
ICE 2005	150	1232
CASIA-IrisV4-Thousand	468	2555
IDDS:NC	118	354
IDDS:Dilation-drugs	19	251
IDDS:Dilation-light	20	41
IDDS:Constriction-drugs	11	218
IDDS:Constriction-light	60	199

3.2. Iris Recognition Systems

Tests are carried out using two different open source iris recognition systems: OSIRISv4.1 [9] and USITv1.0.3 [10]. Since OSIRISv4.1 uses ICE 2005 as the reference data set as is used in this work, it is used as a reference system here.

It should be noted that the iris recognition systems are not optimised for each of the data sets used. For the sake of reproducibility, minimum changes to the original implementations have been made, and these correspond to changes needed to make results comparable. While this might result in increased bit errors, it does not affect the analysis of the consistency of bits in iris codes.

9

3.2.1. OSIRIS v4.1

OSIRISv4.1 (Open Source for Iris version 4.1) is an open source iris recognition system based on Daugman's works [13]. The segmentation stage uses a Viterbi algorithm [14] and Daugman's rubber-sheet model [13] is used to normalise the image. The feature extraction stage is based on Gabor phase demodulation. Each iris code is saved as a binary image of size $W \times (n \times H)$, where $W \times H$ is the size of the normalised image, and n is the number of Gabor filters. In fact, there are $n/2$ Gabor filters, with real and imaginary parts, but OSIRISv4.1 considers the real and imaginary parts as two independent filters. In the comparison stage, irides are compared using the normalised Hamming distance. However, not all the pixels of the iris code are used to perform the comparison. For flexibility purposes, a matrix of 256 application points is used to indicate which pixels are considered. The EER of OSIRISv4.1 with ICE 2005 using the parameters described in [9] is 1.10%.

Some modifications were made to compute the mean normalised bit error. In the original implementation, the effective size of the iris code is 256 bits. Since 12 iris parts (rings and sectors) are used to perform the experiments, the size of the iris code of each of the parts would be only 21 bits. To obtain better estimates of the mean normalised bit error, the entire iris code is used instead of the 256 application points. Other parameters were configured in OSIRISv4.1 as follows. The size of the normalised image is 512×72. Following the recommendations in [15], feature extraction is performed using a bank of filters consisting of the imaginary part of 6 Gabor filters with three different frequencies and two scales. The size of the iris code obtained as a result of binary quadrature encoding is then $512 \times 72 \times 6$. Since the number of bit errors is normalised by dividing over the total number of bits that are compared, the size of the iris codes does not necessarily need to be the same for all systems. Further, iris code representation can be adapted for any system to guarantee that bits within a ring or sector remain in the same ring or sector regardless of the number of filters used.

3.2.2. USIT v1.0.3

USIT (University of Salzburg Iris Toolkit v1.0) is a Windows/Linux software package for iris recognition, made publicly available together with [10]. It comprises different algorithms for iris pre-processing, feature extraction, and comparison. In this case, the starting point are the same normalised iris images as those used with OSIRISv4.1, which have a size of 512×72. Each normalised iris image is divided into stripes to obtain 9 one-dimensional signals, each one averaged from the pixels of 8 adjacent rows (note that in the original implementation of USIT the size of the normalised image is 512×64 and 10 one-dimensional signals are obtained from averaging the pixels of 5 adjacent rows). In order to check the effect of the filter type and encoding on the distribution of bit errors within the iris, two conventional algorithms are employed in the feature extraction stage: a re-implementation of the algorithm proposed by Masek [16] based on 1-D log-Gabor feature extraction, and a re-implementation of the algorithm proposed by Ma *et al.* [17] based on a quadratic spline wavelet transform.

– *Log-Gabor based feature extraction.* In this approach, the nine 1-D intensity signals mentioned above are convolved with a 1-D log-Gabor filter. The phase response at each pixel specifies the coordinates of a phasor in the complex plane. During phase encoding, the angle of each phasor is quantised to one of the four quadrants, setting two bits of phase information. As a result, a $512 \times 2 \times 9$ bit iris code is obtained.

– *Quadratic spline based feature extraction.* A 1-D quadratic spline wavelet transform is applied in this case to the nine 1-D intensity signals mentioned above. Position sequences of detected maxima and minima (local sharp variation points) from two specific sub-bands serve as features. More specifically, sequences of 1s and 0s are assigned to the iris code until new maxima and minima are found. A $512 \times 2 \times 9$ bit iris code is obtained as a result.

11

3.3. Distribution of Bit Errors using the Reference Database and Iris Recognition System

The mean normalised bit error between iris codes of different iris parts can be calculated using equation (1) for any given database and iris recognition system. In this research, bit errors are calculated for 12 radial parts or rings $(\bar{\epsilon}_r^i, i = 1, \ldots, 12)$ and 12 angular parts or sectors $(\bar{\epsilon}_\theta^j, j = 1, \ldots, 12)$, as defined in Fig. 2. The mean normalised bit error obtained for the whole reference data set (ICE 2005) using the reference iris recognition system (OSIRISv4.1) is shown in Fig. 4 for the genuine and impostor distributions.

According to Fig. 4, the distribution of the mean normalised bit error obtained from *impostor* comparisons can be considered uniform and almost equal to 0.5 for radial partitions or rings, as well as angular partitions or sectors. This result is consistent with the fact that if two irides are from different identities, they are expected to have statistically independent iris codes [18] and the expected fraction of agreeing or disagreeing bits between two independent iris codes is 0.5. For *genuine* comparisons, rings nearer the pupil and those nearer the limbus are affected more by bit errors than those in the middle (see Fig. 4a). When considering angular partitioning, sectors around 90° are the most affected
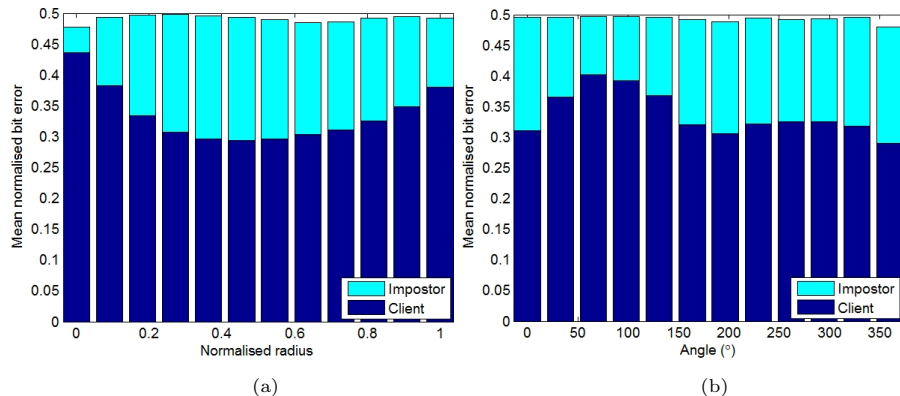

Figure 4: Mean normalised bit error as a function of the (a) radius and (b) angle for genuine and impostor distributions using the whole reference data set (ICE 2005) and dividing the images into 12 rings and 12 sectors respectively.

by bit errors (see Fig. 4b). This behaviour may be attributed to segmentation errors, which are especially prevalent in the eyelid area. Since this work focuses on analysing how the consistency of bits in iris codes differ from one sample to another for the same identity, genuine comparisons are of more interest. From here on, only genuine comparisons will be analysed.

4. Factors Affecting the Distribution of Bit Errors Within the Iris

Using ICE 2005 and OSIRISv4.1 as the reference data set and reference iris recognition system, a V-shaped radial trend of decreasing bit errors towards the central region of the iris is obtained for genuine comparisons, and it is observed that the distribution of bit errors as a function of angle peaks in the upper eyelid area. Some factors have been previously demonstrated [4, 7, 8] to affect such distribution. Using the proposed methodology, an extended list of the factors that are more likely to influence the spatial distribution of bit errors is considered, and a thorough and systematic analysis is carried out to quantitatively assess their effect. The factors that are analysed in this section are: segmentation, capture sensor, resampling, input iris image resolution, filter type and encoding scheme, and changes in pupil size.

4.1. Effect of Segmentation

One of the most common sources of error in iris recognition is imperfect segmentation. In order to check how segmentation errors affect the distribution of bit errors, images from the reference database (ICE 2005) are automatically segmented as described in Subsection 3.2.1 for OSIRISv4.1, and then subjected to a manual selection process to retain only those that are correctly segmented. A manual segmentation process is then performed to refine the mask and eliminate residual errors to the extent possible. After the selection process, a segmentation-error-free reference subset is obtained which includes 1232 images (see Table 1).

13

For analysis purposes, the difference between the bit error distributions corresponding to the whole data set vs. the segmentation-error-free subset can be seen in Fig. 5 for the genuine distribution.

According to Fig. 5a, eliminating segmentation errors reduces the mean normalised bit error per ring up to 0.038 (3.8%) on average, but it does not alter their distribution as a function of the radius. On the contrary, *the effect of segmentation on the angular distribution of bit errors is more noticeable*. According to Fig. 5b, the mean normalised bit error calculated for different sectors using the segmentation-error-free reference subset is almost uniform, and the average equals 0.3 (30%). Therefore, the peak bit error that can be observed around 90° when the whole database is used (see cyan bars) and the trends towards and away from this peak, are mainly due to segmentation errors. These segmentation errors arise in the upper part of the iris, where occlusions due to eyelids and eyelashes are more common.

From here on, the result shown in Fig. 5 for the segmentation-error-free reference subset will be used as the reference bit error distribution. In order to validate the previous result and obtain statistical confidence, repeated random sub-sampling based validation is used. Three quarters of the iris samples from the segmentation-error-free subset are randomly selected and 100 such Monte
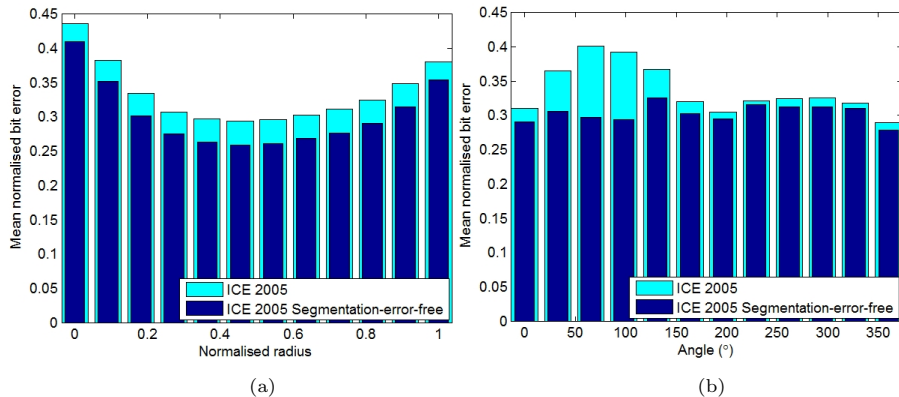

Figure 5: Mean normalised bit error as a function of the (a) radius and (b) angle calculated from genuine comparisons using the whole reference data set and the segmentation-error-free reference subset.

14

Carlo trials are used to compute statistics. Results are shown in Fig. 6 with the standard deviation for each ring and sector represented as an error bar above and below the mean values in each case.

According to the results, *the V-shaped trend for radial partitions or rings is statistically significant*, and any deviation from a uniform error distribution for angular partitions or sectors is not statistically significant. The maximum standard deviation when considering radial partitioning occurs for the middle ring (ring 6) and is equal to 0.0055. The mean value for the standard deviation is 0.0048. In the case of angular partitioning, a maximum standard deviation of 0.011 occurs for sectors around 90°. The mean value for the standard deviation in this case is equal to 0.0069. The maximum standard deviation in the angular case may be arising from minor imperfections that remain even in the trimmed reference subset presumed free of segmentation errors. The reference bit error distribution shown in Fig. 6 in a bar diagram is mapped to a schematic iris in Fig. 7.
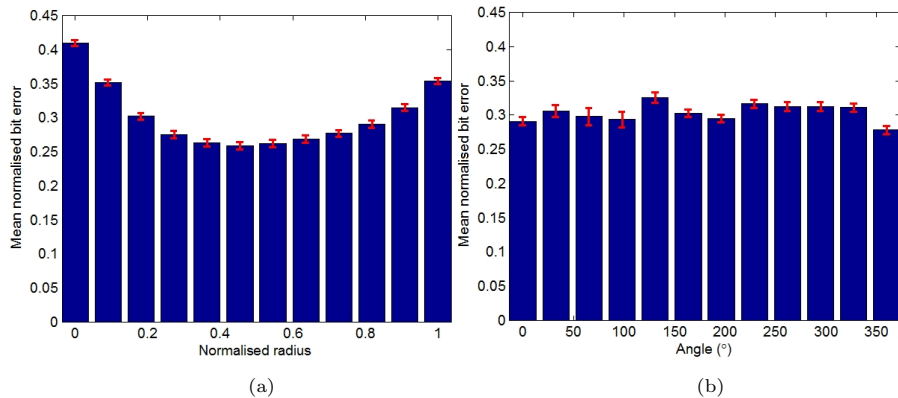

(a)   (b)

Figure 6: Mean normalised bit error as a function of the (a) radius and (b) angle calculated from *genuine* comparisons using the *segmentation-error-free reference* subset. The error bars are one standard deviation. This will be considered the reference distribution of bit errors in the rest of the experiments.
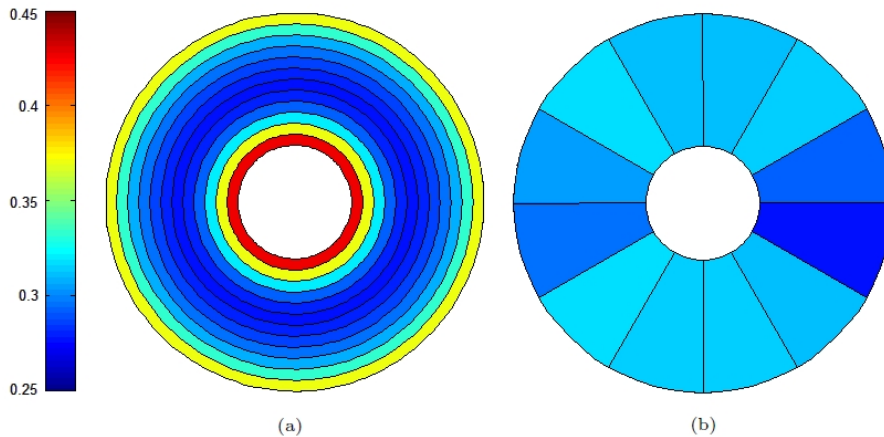
Figure 7: Mean normalised bit error as a function of the (a) radius and (b) angle calculated from *genuine* comparisons using the *segmentation-error-free reference* subset, mapped to a schematic iris.

4.2. Effect of the Capture Sensor

To investigate whether the distribution of bit errors is biased by the particular sensor used to capture the iris images, images from three data sets captured with different iris sensors are considered in this test. Such data sets are ICE 2005, CASIA-IrisV4-Thousand, and IDDS:NC (see Subsection 3.1 for details about the databases and iris sensors). To exclude the effect of segmentation from the results, segmentation-error-free images from each data set are considered (see Table 1). It should be noted that the iris images in the three data sets were acquired from different populations, so some effect of the test population on the results cannot be eliminated. The comparison between the mean normalised bit error computed as a function of the radius and the angle for the three trimmed data sets is shown in Fig. 8.

According to Fig. 8a, a very similar radial distribution of bit errors is obtained for all three databases. Rings 4 to 6 are the least affected by bit errors, and rings nearer to the pupil and limbus are the most affected. Results from Fig. 8b show that bit errors are not distributed exactly the same way for each of the three databases with respect to angular variation, although the distribution is quite uniform in all cases. Bit errors fluctuate around a clearly defined aver-
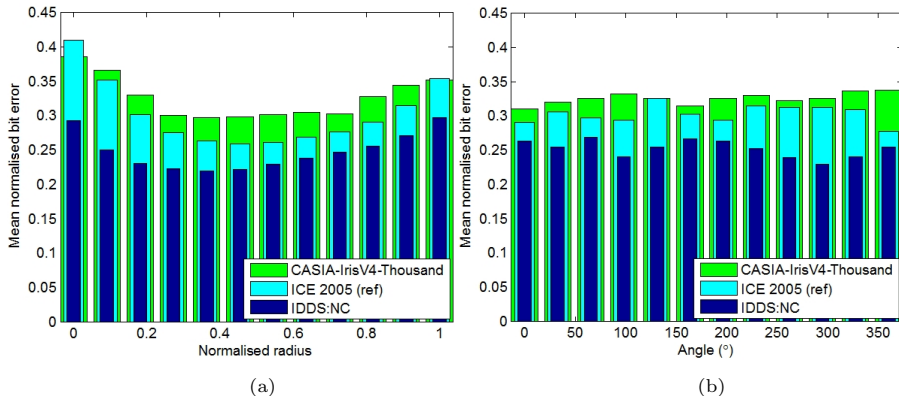
16

Figure 8: Mean normalised bit error as a function of the (a) radius and (b) angle calculated from genuine comparisons using the segmentation-error-free images from three databases that use different iris sensors: ICE 2005, CASIA-IrisV4-Thousand, and IDDS:NC.

age (0.32 for CASIA-IrisV4-Thousand, 0.3 for ICE 2005 and 0.25 for IDDS:NC), with variations that never exceed 0.03. The fact that IDDS:NC shows the lowest mean normalised bit error with the same input image resolution as ICE 2005 and CASIA-IrisV4-Thousand is due to the fact that IDDS:NC images were captured under more ideal conditions. From this experiment it can be concluded that *using different input sensors and different populations results in data exhibiting different mean normalised bit error, but does not affect the general trend of the radial or angular distributions of bit errors.*

4.3. Effect of Resampling

In iris recognition, once the pupil and iris boundaries are located, an iris normalisation process is carried out to map the annular iris region to a rectangular block of fixed dimensions. Iris normalisation is performed in order to counteract changes in the size and scale of the iris patterns. As described by Daugman in [13], invariance to these factors can be achieved by remapping the iris image from Cartesian coordinates to a doubly dimensionless pseudo-polar coordinate system (see Fig. 9).

According to Daugman's rubber sheet model, the remapping of the iris image $I(x(r,\theta), y(r,\theta)) \longrightarrow I(r,\theta)$ can be represented according to equation (2),
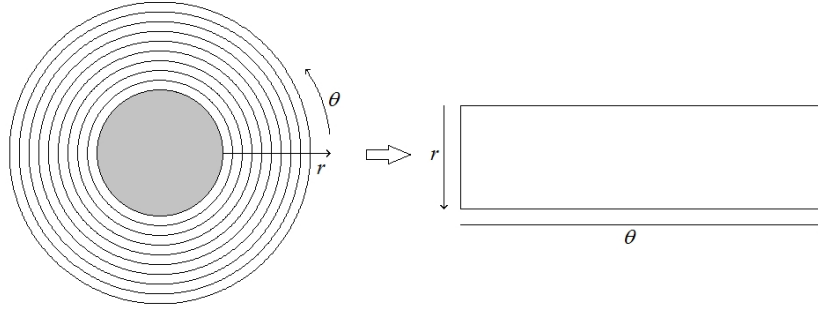
17

Figure 9: Iris normalisation according to Daugman's rubber sheet model [13].

where $(x_p(\theta), y_p(\theta))$ and $(x_s(\theta), y_s(\theta))$ are the discrete coordinates nearest to the pupillary and limbic boundaries, respectively, at a given angle $\theta \in [0, 2\pi]$, and r is the normalised radius in the interval $[0, 1]$.

$$
\begin{aligned}
x(r, \theta) &= (1 - r)\ x_p(\theta) + r\ x_s(\theta), \\
y(r, \theta) &= (1 - r)\ y_p(\theta) + r\ y_s(\theta).
\end{aligned}
\tag{2}
$$

Normalisation involves a resampling process. In the original image, circumferences with different radii have different numbers of pixels, and the distance from the pupillary boundary to the limbic boundary is different for different pupil sizes. However, the normalised image has a constant width and a constant height. The effect of resampling on the distribution of bit errors is investigated by changing the size of the normalised image. Using the reference iris recognition system (OSIRISv4.1), the iris area in the raw iris image is remapped to a normalised rectangular image with fixed dimensions of 512×72 using equation (2). For this test, the reference size of the normalised image is kept the same (512×72) and the distribution of bit errors is checked for smaller and bigger heights (512×36 and 512×144) and widths (256×72 and 1024×72).

By progressively changing the normalised image height it is possible to determine the radial influence of resampling. Results of the mean normalised bit error as functions of the radius and the angle are shown in Fig. 10 for the three sizes under analysis: 512×36, 512×72 (reference) and 512×144.

Since the normalised image height is related only to the iris radius, height changes have only a minor effect on the angular distribution of bit errors (see Fig. 10b), with variations from the reference under 0.035. Nevertheless, they have a minor effect on the radial distribution of bit errors too (see Fig. 10a), and the biggest variation with respect to the reference is equal to 0.039. The results obtained indicate that height resampling hardly has any influence on the distribution of bit errors. It is revealing that *changes in the height of the normalised image do not produce a noticeable change in the mean normalised bit error for radial partitioning.*

In order to determine the angular influence of resampling, the width of the normalised image is progressively changed, as 256×72, 512×72 (reference) and 1024×72. Fig. 11 shows the result of this experiment. According to the results, the distribution of bit errors when considering radial and angular partitioning is the same for the three cases. However, unlike the previous case, *changing the width of the normalised image has a noticeable effect on the mean normalised bit error.* The worst performance is obtained when doubling the reference width, with variations from the reference error equal to 0.055 on average. The fact that
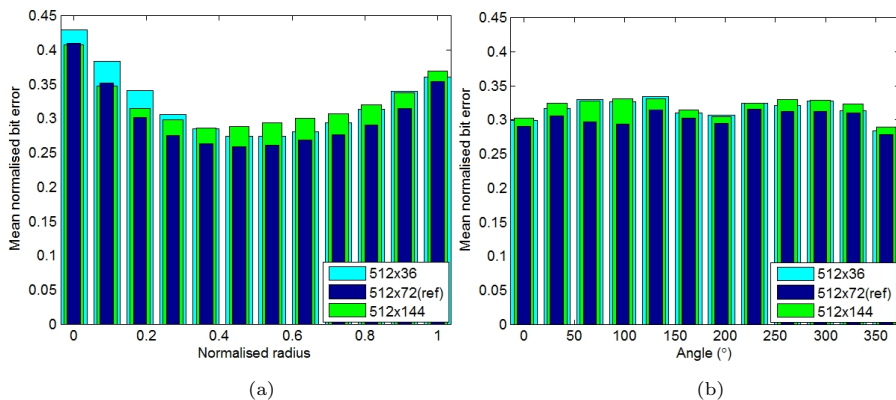

Figure 10: Mean normalised bit error as a function of the (a) radius and (b) angle calculated from genuine comparisons using the segmentation-error-free reference subset with different normalised image heights: 512×36, 512×72 (ref) and 512×144. Test used to check the radial influence of resampling in the distribution of bit errors.
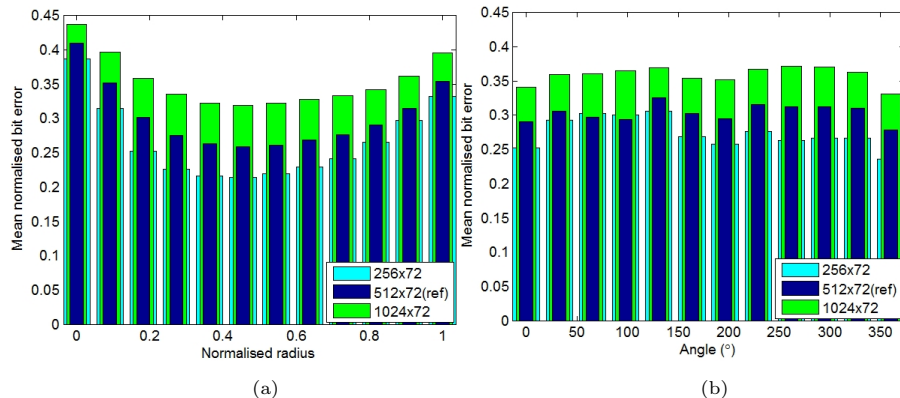
19

Figure 11: Mean normalised bit error as a function of the (a) radius and (b) angle calculated from genuine comparisons using the segmentation-error-free reference subset with different normalised image widths: 256×72, 512×72 (ref) and 1024×72. Test used to check the angular influence of resampling in the distribution of bit errors.

the lowest mean normalised bit error is obtained for a size of the normalised image equal to 256×72 suggests that such size is more suitable since it leads to a better performance.

4.4. Effect of Input Iris Image Resolution

Image resolution is a key factor in iris recognition since poor resolution of the iris significantly degrades the performance. Iris image resolution depends on the specific capture sensor, and also on the distance between the user and the sensor. Robustness to iris size changes due to the distance between the user and the sensor can be achieved by normalisation.

The effect of the resolution of the input iris image on the distribution of bit errors is determined by using different resolution inputs and normalising them to the same pixel grid for further processing. For this test, the resolution of all the segmentation-error-free images in the reference iris data set is changed from 640×480 to 320×240. The images from the segmentation-error-free reference subset and the lower resolution subset are normalised to the same size (512×72) and processed in the same manner. The mean normalised bit error is
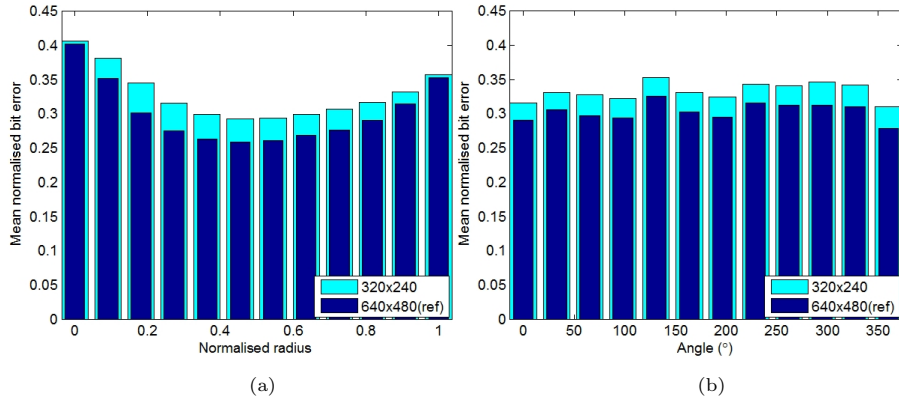
Figure 12: Mean normalised bit error as a function of the (a) radius and (b) angle calculated from genuine comparisons using the input iris images from the segmentation-error-free reference subset at two different resolutions: 320×240 and 640×480 (ref).

then computed and compared. Results are shown in Fig. 12. According to the results, the distribution of bit errors is of the same shape in both cases for both radial and angular partitions, however, the mean normalised bit error increases for the lower resolution images. This result is consistent with the loss of texture detail from lowering the resolution. From this experiment it can be concluded that *the lowest mean normalised bit error is obtained for the database with the highest resolution input images.*

4.5. Effect of Filter Type and Encoding Scheme

Another important factor that might affect the distribution of bit errors within the iris is the filter used to obtain the binary iris codes required to compute the error. To investigate the effect of the feature extraction filter on the distribution of bit errors within the iris, the mean normalised bit error is calculated using two iris recognition systems which use three different types of filter. These are OSIRISv4.1 and USITv1.0.3. As detailed in Subsection 3.2, the first system is configured to use a bank of 2-D Gabor filters for feature extraction, whereas the second one uses 1-D log-Gabor filters (Masek's algorithm) and 1-D quadratic spline filters (Ma's algorithm). It should be noted that while

21

OSIRISv4.1 and Masek's algorithm use phase encoding, Ma's algorithm changes from a sequence of 1s to a sequence of 0s every time a local sharp variation point (maxima or minima) is found, so some effect of the encoding scheme on the results cannot be eliminated. As in all the previous tests, only the segmentation-error-free images from the reference iris data set are used.

The difference between the mean normalised bit errors calculated with the three filters is shown in Fig. 13. According to Fig. 13a, a very similar shaped radial distribution of bit errors is obtained in all cases. Rings 4 to 8 are the least affected by bit errors, and rings closer to the pupil and the limbus are the most affected. The angular distributions of bit errors shown in Fig. 13b are not exactly the same but are quite uniform in all cases. The mean normalised bit error fluctuates around a clearly defined average (0.33 for 1-D quadratic spline filter, 0.3 for 1-D log-Gabor filter, and 0.3 for 2-D Gabor filter) with variations that never exceed 0.024. From this experiment it can be concluded that *using different filters (Gabor, log-Gabor and quadratic spline filters in this case) and encoding schemes (encoding based on local variation points and phase encoding) results in data exhibiting different mean normalised bit error, but does not affect the general trend of the radial or angular distributions of bit errors.*
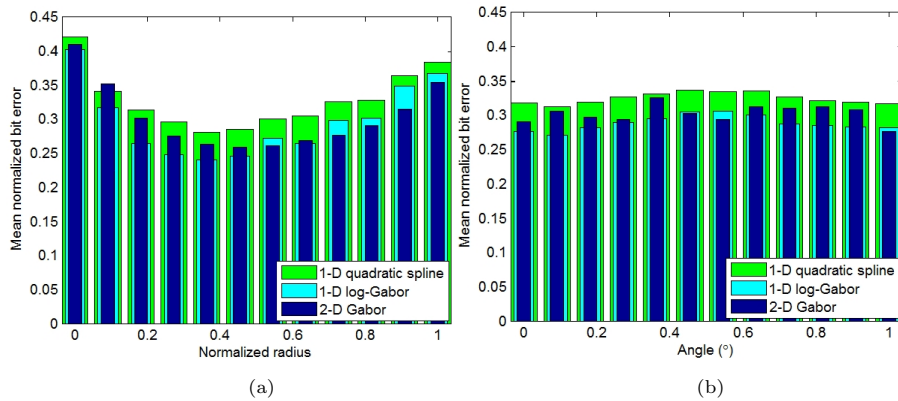

Figure 13: Mean normalised bit error as a function of the (a) radius and (b) angle calculated from genuine comparisons using the segmentation-error-free reference subset with two iris recognition systems that use three different filters: 1-D quadratic spline filter, 1-D log-Gabor filter, and 2-D Gabor filter.

4.6. Effect of Changes in Pupil Size

In [4] and [7], the authors hypothesise about the effect of pupil dilation on the consistency of the inner regions of the iris, but no experiments are presented to test this hypothesis. In [19], bit error analysis was used to investigate and compare the effects of light and drug induced pupil dilation and constriction considering various degrees of dilation. New results for the mean normalised bit error are calculated here for images affected by drug-induced and light-induced pupil dilation and constriction, without differentiating between dilation degrees.

To analyse the effect of pupil dilation on the distribution of bit errors within the iris, the mean normalised bit error is calculated for images affected by drug-induced pupil dilation (IDDS:Dilation-drugs) and light-induced pupil dilation (IDDS:Dilation-light) when comparing them with the corresponding templates captured under normal conditions (IDDS:NC). The result of this comparison is shown in Fig. 14.

According to Fig. 14a, the V-shaped trend obtained for radial partitions or rings disappears when the iris is affected by drug-induced pupil dilation. Due to the smaller amount of iris area visible and the degradation of iris texture detail, bit errors are distributed in a more uniform way, although the four rings nearer
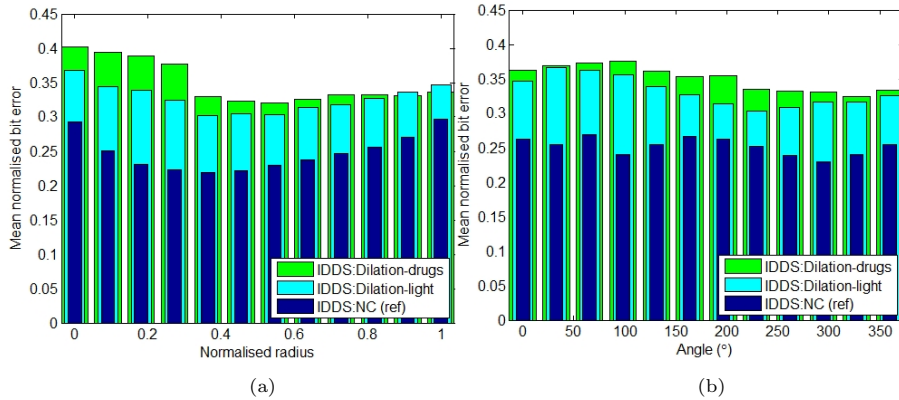

Figure 14: Mean normalised bit error as a function of the (a) radius and (b) angle calculated from genuine comparisons using the images from the IDDS light-induced and drug-induced pupil dilation subsets (IDDS:Dilation-light and IDDS:Dilation-drugs), and their counterparts under normal conditions (IDDS:NC).

23

to the pupil are clearly more affected by the dilation and show an increased number of errors. In the case of light-induced pupil dilation, the original V-shaped trend is not totally lost, but slightly displaced towards more outer rings of the iris. This displacement suggests that the *inner rings of the iris are more severely affected by pupil dilation.* The distributions of bit errors for angular partitions or sectors shown in Fig. 14b are quite uniform in all cases, although a small increase in the mean normalised bit error can be observed in sectors between $50°$ and $150°$. This may be arising from the minor imperfections that remain after manual mask refinement.

In agreement with previously reported results in which pupil dilation is demonstrated to affect iris recognition performance [20, 21], the graphs in Fig. 14 clearly show that the mean normalised bit error increases considerably when matching iris images with large differences in pupil size. Since pupil dilation reduces the amount of iris area visible, there is less information (fewer pixels) to characterise the texture of the iris. This increases the number of bit errors. Compared with the reference case in which images are captured under normal conditions and show normal pupil sizes, the mean normalised bit error increases on average by 0.104 (10.4%) for drug-induced pupil dilation and by 0.086 (8.6%) for light-induced pupil dilation. This result indicates that *the effect of mydriatic drugs on the iris texture is more severe than the effect provoked by the absence of light.* The difference between drug- and light-induced pupil dilation is especially noticeable in those rings closer to the pupil. This correlates well the fact that the mydriatic agent instilled to the users (1% tropicamide) leads to the paralysis of the sphincter iris muscle [22] located in the pupillary area.

To investigate the effect of pupil constriction on the consistency of bits in iris codes, and check whether there are relevant differences between pupil dilation and constriction, the mean normalised bit error is computed as a function of the iris radius and angle. Fig. 15 shows the bit error distributions of images affected by drug-induced pupil constriction (IDDS:Constriction-drugs) and light-induced pupil constriction (IDDS:Constriction-light) when comparing them with the corresponding templates captured under normal conditions (IDDS:NC).
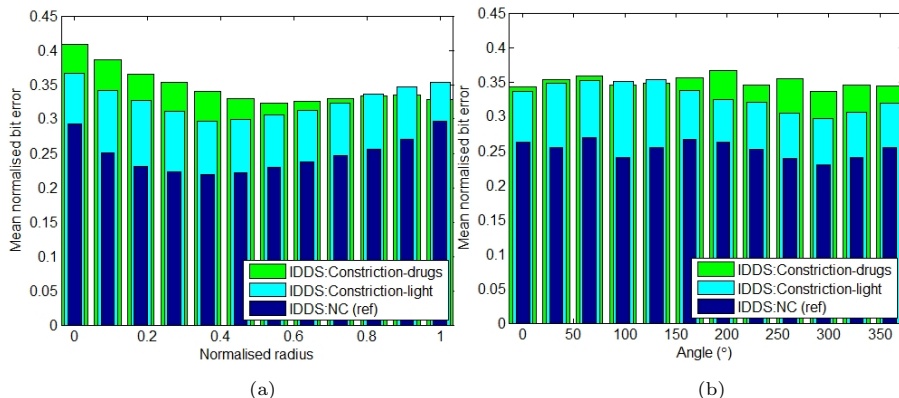
Figure 15: Mean normalised bit error as a function of the (a) radius and (b) angle calculated from genuine comparisons using the images from the IDDS light-induced and drug-induced pupil constriction subsets (IDDS:Constriction-light and IDDS:Constriction-drugs), and their counterparts under normal conditions (IDDS:NC).

Results in Fig. 15a show that *for drug-induced constriction the bit errors show a decreasing trend from the pupil outwards rather than a V-shaped trend.* In the case of light-induced pupil constriction, the radial bit error distribution retains characteristics of the V-shaped trend of the reference data, although it gets stretched up near the pupil. Fig. 15b shows that the mean normalised bit error as a function of the angle retains the uniform distribution. The increase in the number of bit errors when images are affected by pupil constriction is due to the fact that some of the texture information that becomes available when the pupil constricts is not available in the reference images, which are captured under normal conditions and show normal pupil sizes. On average, the mean normalised bit error increases by 0.098 (9.8%) for drug-induced pupil constriction and by 0.078 (7.8%) for light-induced pupil constriction. As in the case of dilation, *bit errors arising from drug-induced pupil constriction are higher than those arising from light-induced pupil constriction* (2% higher on average). The effect of the miotic agent on the iris muscles might be the cause of this.

A more detailed analysis of the effect of drug and light induced changes in pupil size on the distribution of bit errors within the iris can be found in [19].

5. Conclusion

The distribution of bit errors in iris codes as functions of radius (ring) and angle (sector) for a range of factors is analysed in this work more comprehensively than previous studies of consistency of iris codes. Three data sets and two open source iris recognition systems have been used in the study. The effect of segmentation errors is first checked and then eliminated manually to ensure that all segmentation and masking is as accurate as possible. Images free from segmentation errors are used to investigate the effects of other factors. Factors investigated in this work include different capture sensors, image resolutions, feature extraction and encoding algorithms, and pupil sizes. In general, results confirm the trend observed in previous studies for images where the pupil size is normal. The mean normalised bit error for genuine comparisons increases as a function of the radius towards both the pupillary and limbic boundaries (V-shaped trend). This study makes additional observations. The V-shaped trend is found not to be significantly changed regardless of the capture sensor, re-sampling, image resolution, filter and encoding algorithm. The only factor that destroys the V-shaped bit error distribution as a function of radius is a significant pupil size change in the form of dilation or constriction. Both dilation and constriction result in increased bit errors, especially in the pupillary area. Drug induced changes are found to be more pronounced than light induced changes. They increase the mean normalised bit error and make the radial distribution of errors more uniform. The mean normalised bit error distribution as a function of angle is found to be essentially uniform regardless of the factor investigated with a small decrease in the errors towards sectors closer to the eye corners.

References

[1] P. J. Grother, G. W. Quinn, J. R. Matey, M. L. Ngan, W. J. Salamon, G. P. Fiumara, C. I. Watson, IREX III - Performance of iris identification algorithms, Tech. rep., NIST Interagency/Internal Report (NISTIR) 7836 (2012).

[2] M. B. Pereira, A. C. P. Veiga, A method for improving the reliability of an iris recognition system, in: IEEE Pacific Rim Conference on Communications, Computers and Signal Processing, 2005, pp. 665–668.

[3] M. B. Pereira, A. C. P. Veiga, Application of genetic algorithms to improve the reliability of an iris recognition system, in: Workshop on Machine Learning for Signal Processing, 2005, pp. 159–164.

[4] K. P. Hollingsworth, K. W. Bowyer, P. W. Flynn, The best bits in an iris code, IEEE Transactions on Pattern Analysis and Machine Intelligence 31 (6) (2009) 964–973.

[5] C. Rathgeb, A. Uhl, P. Wild, Incremental iris recognition: A single-algorithm serial fusion strategy to optimize time complexity, in: IEEE International Conference on Biometrics: Theory, Applications and Systems, 2010, pp. 1–6.

[6] C. W. Tan, A. Kumar, Adaptive and localized iris weight map for accurate iris recognition under less constrained environments, in: IEEE International Conference on Biometrics: Theory, Applications and Systems, 2013.

[7] R. P. Broussard, L. R. Kennell, R. W. Ives, Identifying discriminatory information content within the iris, in: SPIE 6944, Biometric Technology for Human Identification, 2008.

[8] A. Hilal, P. Beauseroy, B. Daya, Advances in Systems Science, Advances in Intelligent Systems and Computing, Vol. 240 of Advances in Intelligent Systems and Computing, Springer International Publishing, 2014.

[9] G. Sutra, B. Dorizzi, S. Garcia-Salicetti, N. Othman, A biometric reference system for iris, OSIRIS version 4.1 (2012).

[10] C. Rathgeb, A. Uhl, P. Wild, Iris Recognition: From Segmentation to Template Security, Vol. 59 of Advances in Information Security, Springer, New York, 2012.

[11] ICE 2005 Database.
URL http://iris.nist.gov/ice/

[12] CASIA-IrisV4.
URL http://biometrics.idealtest.org

[13] J. G. Daugman, High confidence visual recognition of persons by a test of statistical independence, IEEE Transactions on Pattern Analysis and Machine Intelligence 15 (11) (1993) 1148–1161.

[14] G. Sutra, S. Garcia-Salicetti, B. Dorizzi, The Viterbi algorithm at different resolution for enhanced iris segmentation, in: International Conference on Biometrics, 2012, pp. 310–316.

[15] L. Ma, Y. Wang, T. Tan, Iris recognition based on multichannel gabor filtering, in: Asian Conference on Computer Vision, 2002.

[16] L. Masek, Recognition of human iris patterns for biometric identification, Master's thesis, School of Computer Science and Software Engineering, University of Western Australia (2003).

[17] L. Ma, T. Tan, Y. Wang, D. Zhang, Efficient iris recognition by characterizing key local variations, IEEE Transactions on Image Processing 13 (6) (2004) 739–750.

[18] J. G. Daugman, The importance of being random: Statistical principles of iris recognition, Pattern recognition 36 (2) (2003) 279–291.

[19] I. Tomeo-Reyes, V. Chandran, Effect of pupil dilation and constriction on the distribution of bit errors within the iris, in: IEEE International Conference on Computer Vision and Pattern Recognition Workshops, 2014.

[20] K. Hollingsworth, K. W. Bowyer, P. W. Flynn, Pupil dilation degrades iris biometric performance, Computer Vision and Image Understanding 113 (1) (2009) 150–157.

[21] O. Seyeddain, H. Kraker, A. Redlberger, A. K. Dexl, G. Grabner, M. Emesz, Reliability of automatic biometric iris recognition after phacoemulsification or drug-induced pupil dilation, European Journal of Ophthalmology 24 (1) (2014) 58–62.

[22] M. G. Rajanandh, M. S. P. Kumar, V. Chaparla, R. Teja, N. N. K. Chakravarthi, J. J. Molekunnel, C. Ramasamy, Mydriatic effect of tropicamide, proparacaine and lignocaine: A mono and combination therapy, International Journal of Pharma and Bio Sciences 2 (3) (2011) 128–132.

Author Biographies

Inmaculada Tomeo-Reyes received the M.E. and B.E. degrees in Telecommunications Engineering from Universidad Carlos III de Madrid (UC3M, Spain) in 2008 and 2006, respectively. She received the M.S. degree in Multimedia and Communications from UC3M in 2010, and the Ph.D. degree in Electrical Engineering from Queensland University of Technology (QUT, Australia) in 2015. Her research interests include signal and image processing, pattern recognition, machine learning, and biometrics. She is currently an Associate Lecturer at QUT.

Vinod Chandran holds a Ph.D. (1990) from Washington State University, USA. He has Masters Degrees in Electrical Engineering from Texas Tech University in 1985 and Computer Science from Washington State University in 1991. He graduated with a B. Tech in Electrical Engineering from IIT Madras, in 1982. He is currently a Professor at Queensland University of Technology, Australia. His research interests are signal processing, image processing and pattern recognition for biometrics and biomedical applications. He has co-authored over 160 peer-reviewed publications.